J. Physiol. (1974), **239**, *pp.* 301–324
With 1 plate and 8 text-figures
Printed in Great Britain

SPECIFIC MEMBRANE PROPERTIES OF CAT MOTONEURONES

BY J. N. BARRETT* AND W. E. CRILL

From the Departments of Physiology and Biophysics and Medicine, University of Washington School of Medicine, Seattle, Washington 98195, U.S.A.

(*Received 18 January 1973*)

SUMMARY

1. Electrophysiological properties of cat motoneurones were measured using intracellular electrodes, after which Procion dye was injected iontophoretically into the neurone through the recording pipette.

2. Histological procedures were chosen to minimize changes in neuronal morphology. Reconstructed motoneurones had more dendritic branches and larger surface areas than the Golgi-stained motoneurones of earlier reports.

3. The sum of the 3/2 power of the dendritic diameters (the dendritic trunk parameter; Rall, 1959) of the reconstructed motoneurones was found to decrease with distance from the soma. Thus, the dendritic tree is not satisfactorily approximated by a non-tapering membrane cylinder.

4. A computational technique was developed to allow calculation of the specific resistance (R_m) of the membrane using the measured value of the input resistance of the motoneurone and a more detailed approximation of the dendritic tree. These calculations indicate that the average resting value of dendritic R_m is at least 1800 Ω cm^2. The specific membrane capacity, calculated assuming uniform R_m, ranged between 2–3 μF/cm^2.

INTRODUCTION

Synaptic currents alter the activity of neurones by polarizing the region where action potentials are initiated. In cat motoneurones most synaptic contacts are made on the dendritic tree (Conradi, 1969), and are therefore spatially and electrically removed from the usual spike-initiating region in the axon hillock. The effectiveness of these dendritic synapses depends

* Present address: Department of Physiology, University of Iowa Medical School, Iowa, Iowa City, Iowa, 52240.

upon the passive membrane properties of the post-synaptic cell. If the specific membrane resistance (R_m) is high, a large fraction of the current from distant dendritic synapses will be transmitted electrotonically to the spike-initiating zone, whereas if R_m is low, very little of the current from distant synapses will reach the soma and initial segment.

Earlier studies of cat motoneurones reported estimates of R_m ranging from 500 to 4000 Ω cm^2 (Frank & Fuortes, 1956; Coombs, Curtis & Eccles, 1959; Rall, 1959; Kernell, 1966). This wide range of values is not surprising, since all of these studies used electrical and morphological measurements from different samples of motoneurones. Recently Lux, Schubert & Kreutzberg (1970) recorded the passive voltage responses of single motoneurones to current steps, injected the neurone with tritiated glycine, and subsequently reconstructed the geometry of the cell from serial autoradiographs. Their calculations, which approximated the dendrites as finite equivalent cylinders, set the average electrotonic length of these equivalent cylinders at 1·5 space constants and the average R_m at 2700 Ω cm^2.

In the experiments described here, the passive electrical properties of cat motoneurones were measured, after which the same cells were injected with fluorescent Procion dye. Because morphological measurements of the reconstructed neurones failed to justify the equivalent cylinder approximation of the dendrites, we used geometrical reconstructions of each cell to calculate R_m, the electrotonic length L of each dendrite and the dendrite-to-soma conductance ratio. The specific membrane capacity (C_m) was calculated from R_m and the electrical time constant τ_0, and R_m and C_m values were combined with geometrical measurements to predict the detailed shape of the transient voltage response to a step of current injected into the soma.

Preliminary reports of portions of this work have been published (Barrett & Crill, 1971*a*, *b*).

METHODS

Animal preparation. Adult cats (1·5–2·5 kg) were anaesthetized with sodium pentobarbitone (35 mg/kg). After the first 6 hr, the anaesthetic level was maintained with an infusion of approximately 6 mg sodium pentobarbitone/hr. Cats were paralysed with gallamine triethiodide and artificially respired. The posterior tibial, anterior tibial and peroneal nerves were placed on platinum stimulating electrodes in an oil bath. Following a lumbar laminectomy, the dorsal roots of the L 5–S 2 spinal cord segments were cut and deflected to the other side, exposing the spinal cord lateral to the dorsal root entry zone. The temperature of the mineral oil covering the exposed spinal cord and leg nerves was maintained at 37 $\pm$ 0·5° C by small heat lamps. Rectal temperature was maintained at 37 $\pm$ 0·1° C. A bilateral pneumothorax and a device to hold the chest wall expanded improved stabilization of the spinal cord.

Recording procedures. Lumbosacral motoneurones identified by antidromic activation were impaled with bevelled (Barrett & Graubard, 1970) single- or double-barrelled (θ tubing) electrodes filled with Procion dye (5% Procion Yellow in aqueous solution). Micro-electrode resistances ranged from 9 to 20 MΩ in spinal cord. Electrical recordings were made through a unity-gain, high input impedance preamplifier with feed-back compensation for stray capacitance to ground. Current steps were applied through a 10^9 Ω resistor, and a Wheatstone bridge circuit was used to balance the resistance of single-barrelled electrodes or the coupling resistance between current and voltage barrels of double-barrelled electrodes (Nelson & Frank, 1967; Burke & ten Bruggencate, 1971). The bridge circuit was balanced extracellularly, but usually required slight readjustment after neuronal penetration. Intracellular bridge balance was achieved by balancing out the very fast components of the voltage response to a current step (Nelson & Frank, 1967; Purple, 1964). This balance was checked while neuronal input resistance was reduced to a low value by stimulating the dorsal roots at 1 kHz. When only a few millimetres of the double-barrelled pipette tips were filled with electrolyte fluid, the capacitative-coupling artifact lasted less than 0·2 msec.

The input resistance R_N of the resting motoneurone was measured from the steady-state voltage change produced by a depolarizing 1–5 nA current pulse lasting 20–50 msec (Fig. 1). The conduction velocity of the motoneurone axon was calculated from the latency difference of antidromic action potentials evoked from stimulation sites separated by 5–10 cm on the motor nerve.

Staining procedures. Following collection of electrophysiological data, Procion dye was injected iontophoretically from the micro-electrode using a constant hyperpolarizing current of 60–100 nA maintained for 20–45 min (voltage clamped neurones were not injected). Use of bevelled electrodes (Barrett & Graubard, 1970) increased the fraction of successful injections from less than 20% to approximately 70%.

Two to twelve hours after dye injection, the animals were perfused through the descending aorta with phosphate-buffered 4% paraformaldehyde at pH 7·3. The extirpated lumbar spinal cord was stored in this fixative for 12 hr before cutting frozen cross-sections 50–100 μm thick. The final buffer osmolarity of the fixative (450 m-osmole) was chosen to minimize swelling or shrinkage of neurones (Westrum & Lund, 1966), and tissue dimensions showed no detectable alteration during fixation (2% linear accuracy). Damage due to ice crystal formation was reduced by placing the tissue blocks in a solution of the above fixative in 15% glycerol for 20 min before freezing. Direct observation revealed that mounting and clearing procedures employing alcohol dehydration cause up to 50% volume shrinkage of the injected neurones. Therefore, frozen tissue sections were mounted in 95% glycerol, which helped clear the tissue without noticeably changing neuronal dimensions. Motoneurones evidencing histological damage were not used. Tissue sections were examined by standard blue-light fluorescent techniques (460 nm excitation light). Dark-field illumination was often used to reduce background fluorescence. Paraformaldehyde fixative gave lower background fluorescence than gluteraldehyde (see also Stretton & Kravitz, 1968).

Stained cells were matched with electrophysiological records by reference to stereotaxic co-ordinates and marker dyed electrode tracks on the contralateral side of the spinal cord. Each neurone was traced at 600× to 1500× magnification using a camera lucida attachment, and reconstructed from tracings of individual sections. Dendritic diameters were measured at 1500× magnification (resolution ~ 0·5 μm). The length of each dendritic segment was calculated from the projection in the plane of the section and the vertical (depth) projection measured with the calibrated focal adjustment of the microscope and corrected (using Snell's law) for the refractive index of the mounting medium. Calculations used the actual anatomical measurements with no correction factors.

Computational methods

Steady-state calculations. Because the dendritic trunk parameter decreased with distance from the soma (see Results), calculations of input impedance used the detailed geometry of each injected motoneurone. The dendritic tree was broken into 300–700 short segments (5–100 μm in length), each approximated by a cylinder. The length of each segment varied inversely with the rate of tapering in that portion of the dendritic tree, such that the dendritic diameters of the segmented model never differed by more than 0·2 μm from the actual measured diameters, except in the large, rapidly tapering proximal dendrites (within 10–20 μm of the soma), where the tolerance was 0·5–1 μm.

The segmented model was transferred as a coded list of segment lengths and diameters into a PB 440 computer, which calculated the value of the steady-state neuronal input resistance R_N for a given assumed value of R_m by applying eqn. (14) for the case $\omega = 0$ (see Appendix) to successive dendritic segments (see also Rall, 1959). The accuracy of the computer programs was confirmed by applying them to branched, non-tapering dendritic models, for which a direct analytical (equivalent cylinder) solution was available for comparison (Rall, 1959). By using an analytical solution for the input resistance of each segment, instead of approximating the dendrites as a series of isopotential compartments, we avoided any intrinsic computational error due to the finite cable lengths of the segments.

Computations began by calculating the input conductance of the most distal dendritic segments, assuming either sealed or infinite cylinder-termination (see Results). The input conductance of the distal segment specifies the terminating conductance of the next more proximal segment, allowing calculation of the input conductance of that segment, and so forth toward the soma. At branch points the terminating conductance of the parent branch is the sum of the input conductances of the daughter branches. The input conductance at the soma (the reciprocal of its input resistance R_N) is the sum of the input conductances of all the dendrites added in parallel and the input conductance of the soma, the latter calculated from a geometrical approximation of the soma shape.

Calculations of R_N were repeated for R_m values ranging from 500 to 4000 Ωcm^2, to give plots such as that of Fig. 3. The value of R_m that predicts the steady-state input resistance of the whole neurone seen by an electrode in the soma is taken as the average $R_m$of the motoneurone, assuming uniform R_m for all membranes.

Transient calculations. The complex input impedance of the neurones at the soma was calculated at various frequencies (see below) by applying eqns. (12), (13) and (14) (Appendix) to the segmental model of the dendritic tree described above. Calculations employed the average value of R_m (see above) and the longest time constant τ_0 in the electrically recorded response to an applied current step (e.g. Text-fig. 1). Computations at any one frequency followed the iterative procedure outlined above and in the Appendix. At each frequency ω the complex input impedance, $Z(\omega)$, was expressed in polar form as an amplitude $A(\omega)$ and a phase shift $\phi(\omega)$,

$$Z(\omega) = A(\omega)\, e^{j\phi(\omega)}.$$

Calculation of $Z(\omega)$, $A(\omega)$ and $\phi(\omega)$ was repeated for at least 200 frequencies between 0 and $10^5\ \omega\tau_0$ (normalized frequency, see Rall, 1959; ten frequencies between 0 and $0{\cdot}1\ \omega\tau_0$, 160 between 0·1 and $10^3\ \omega\tau_0$, and thirty between 10^3 and $10^5\ \omega\tau_0$), such that for $0 \leqslant \omega\tau_0 < 10^3$ plots of $A(\omega)$ and $\phi(\omega)$ constructed by linear extrapolation between calculated points would not deviate by more than 0·1 % from the actual calculated value at any intermediate frequency.

From these data, the impulse response of the neurone, $h(t)$, was evaluated numerically using the Fourier integration:

$$h(t) = \frac{2}{\pi}\int_0^\infty A(\omega)\cos\theta(\omega)\cos\omega t\,\mathrm{d}\omega. \quad (1)$$

Convolution of $h(t)$ in eqn. (2) yields the voltage response of the neurone, $V(t)$, to current, $I(t)$, applied at the soma:

$$V(t) = \int_0^t h(t-\tau)\,I(\tau)\,\mathrm{d}\tau. \quad (2)$$

The impulse response was also used to predict the transient current response to a voltage step in the voltage-clamp mode, by letting the voltage time course in eqn. (2) be a step at $t = 0$ and solving numerically for $I(t)$.

Certain features of these experimental and analytical techniques are elaborated in Barrett (1973), and related computational techniques are discussed by Norman (1972).

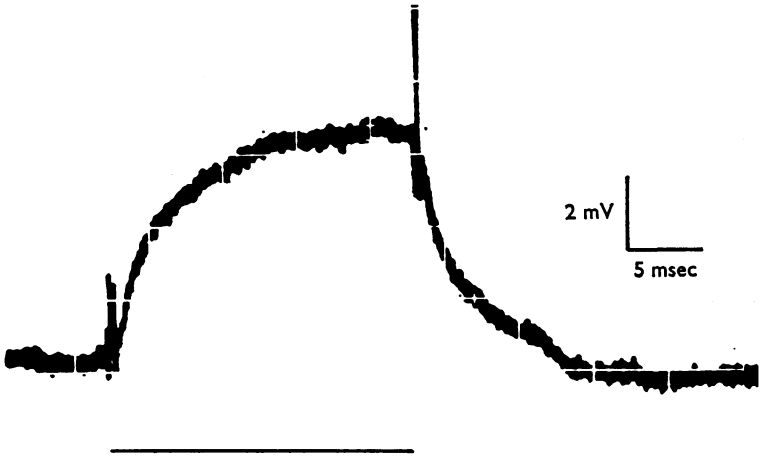

Text-fig. 1. Voltage response recorded from motoneurone 8, during injection of 3 nA current step during the solid bar at bottom of the Figure. Time calibration is 5 msec; voltage calibration is 2 mV. Note slight hyperpolarization after pulse.

RESULTS

Anatomical observations. Text-fig. 2 shows a reconstruction of a dye-injected motoneurone, made by superimposing tracings of dye-filled branches from twelve serial cross-sections. The distal terminal dendritic branches of the injected motoneurones were 300–800 μm from the cell body and had diameters of 1 μm or less. Axons could usually be followed into the ventral white matter adjacent to the ventral grey and, in half the cases, into the ventral root filament. Three of forty stained cells showed axon collaterals branching about 300 μm from the soma. A prominent feature of the motoneurone reconstructions was the variable size of the

dendritic arborizations. Each neurone had eight to twenty-two primary dendritic trunks, and the calculated surface area of the soma and dendrites ranged from 79,000 to 250,000 μm^2. Aitken & Bridger (1961) saw two to fourteen primary dendrites (mean seven for their multipolar neurones) in their Golgi-stained cat ventral horn neurones. Their largest cell had a surface area of 98,000 μm^2. Our injected motoneurones also displayed a greater total dendritic length and a higher dendrite-to-soma surface

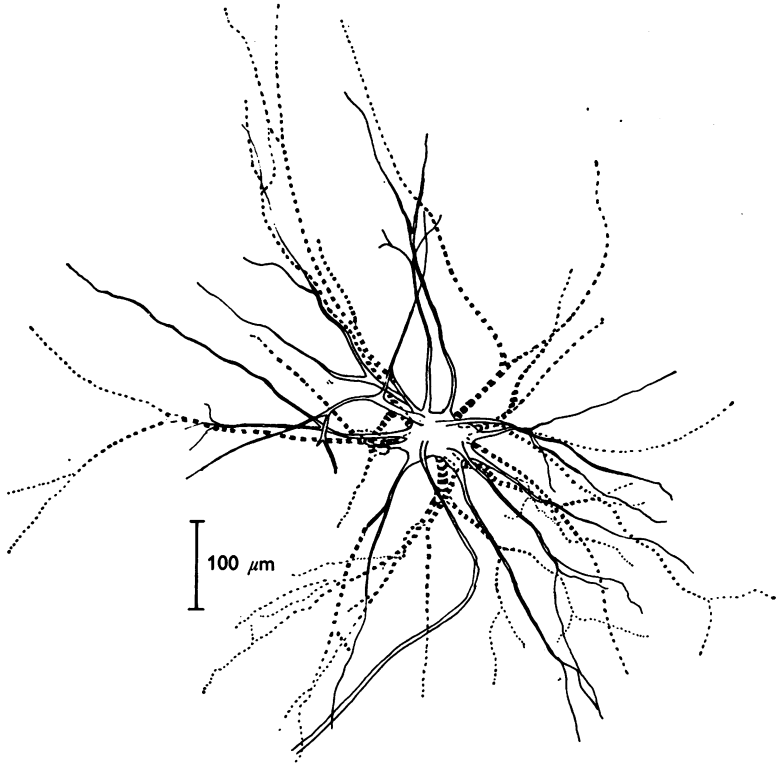

Text-fig. 2. Reconstruction of a Procion-dye injected motoneurone from the medial gastrocnemius nucleus. This is a composite of tracings of dye-filled segments from twelve serial cross-sections, each 100 μm thick. Dashed dendrites are behind the plane of the soma. Scale 100 μm.

area ratio than the Golgi-stained neurones. Histological precautions against cell shrinkage (see Methods) probably account for the larger size of our injected neurones. The intense fluorescence of the injected dendrites allowed us to detect more dendritic branches and to follow dendrites easily from one serial section to the next.

Other investigators have assumed that the more rapidly conducting axons originate from larger motoneurones because of the inverse relation-

ship between input resistance R_N and axonal conduction velocity (Kernell, 1966). The data in Table 1 confirm this: dendritic surface area is positively correlated with axonal conduction velocity (regression correlation coefficient $r = 0{\cdot}61$; $P < 0{\cdot}04$ by t test) and is also inversely related to input resistance ($r = -0{\cdot}79$, $P < 0{\cdot}005$).

Specific membrane properties. In several previous studies, the dendritic tree of motoneurones was approximated as an equivalent cylinder (Rall, 1959; Lux *et al.* 1970). This assumption is valid if the combined dendritic trunk parameter ($\Sigma d^{\frac{3}{2}}$, where d is the diameter of each dendritic branch) does not change with the distance from the soma (Rall, 1959). Lux *et al.* report a decrease in $\Sigma d^{\frac{3}{2}}$ over the proximal 50 μm of the dendritic tree, but suggest no further decrease beyond this distance. Our motoneurone reconstruction also showed a rapid decrease in $\Sigma d^{\frac{3}{2}}$ in the proximal dendritic tree, but, in addition, eight of the ten motoneurones studied in detail exhibited a continuing (although slower) decrease in $\Sigma d^{\frac{3}{2}}$ over the distal dendritic tree as well (Fig. 6, see also Barrett & Crill, 1971*b*). Between 50 and 300 μm from the soma, for example, $\Sigma d^{\frac{3}{2}}$ in these eight motoneurones dropped 22–37·5 %. The two other motoneurones exhibited less than a 5 % decrease in $\Sigma d^{\frac{3}{2}}$ over this distance. Between 0 and 300 μm from the soma most of the decrease in $\Sigma d^{\frac{3}{2}}$ was due to dendritic tapering between branch points (Pl. 1), rather than to loss or termination of dendritic branches. $\Sigma d^{\frac{3}{2}}$ appeared to be preserved at branch points, in agreement with Lux *et al.* The observed overall decrease in $\Sigma d^{\frac{3}{2}}$ with distance was not due to rapid tapering in a few 'anomalous' dendrites; in some motoneurones over 90 % of the individual dendrites exhibited significant tapering between 50 and 400 μm. The observed degree of tapering in the ten motoneurones was not obviously related to the time between dye injection and fixation (i.e. diffusion time); tapering was evident even in neurones allowed 12 hr diffusion time. Beyond 300–400 μm termination of dendritic branches accounted for most of the continued decrease in $\Sigma d^{\frac{3}{2}}$.

Thus, both dendritic tapering between branch points and distributed termination of dendrites caused the dendritic trunk parameter to decrease with distance from the soma in the majority of our motoneurones. Because the dendritic trunk parameter was not constant, we did not use the equivalent cylinder approximation, but rather approximated the dendritic tree as a series of short, branched, interconnected cylinders (see Methods).

To evaluate the relationship between R_N and R_m using eqn. (14), values for the resistivity of the cytoplasm, R_a, and the terminating admittance, Y_T, of the most distal core segments are needed. Previous studies of motoneurones have used values of R_a, ranging from 50 Ω cm (Rall, 1959) to 100 Ω cm (Lux *et al.* 1970). We measured the resistivity of the somatic cytoplasm using the technique of Schanne (1969) and obtained a mean

TABLE 1. Electrophysiological and geometrical data and calculated membrane properties for ten motoneurones that were intensely stained by Procion dye and showed no apparent histological distortion

Cells no.	R_N (MΩ)	Surface area of neurone (μm^2)	Conduction velocity (m/sec)	Time constant (msec)	R_m (Ω cm²)		Dendrite/soma conductance ratio		Mean electrotonic length of dendrites (space constants) (± S.D.)	Number of primary dendrites	Dendritic membrane area / Soma membrane area
					Closed	Infinite	Closed	Infinite			
1	1·03	250,000	117	4·7	1900	2470	10·8	14·5	1·3 ± 0·3	21	15·3
2	1·15	222,000	95	3·2	1300	1950	16	19	1·3 ± 0·2	9	27·3
3	1·26	141,000	107	3·7	1200	1300	9·5	9·6	1·3 ± 0·3	9	13·8
4	1·30	125,000	109	5·0	1420	2500	4·8	9·1	1·3 ± 0·1	7	5·6
5	1·45	179,000	99	7·4	2080	2250	8·6	9·5	1·5 ± 0·3	12	11·2
6	1·72	146,000	92	3·3	1700	2200	10·5	13·8	1·3 ± 0·2	13	16·2
7	2·07	129,000	70	5·2	2100	3550	11·6	21	1·4 ± 0·1	8	15·4
8	2·30	92,100	81	5·5	1650	3050	10	15·7	1·1 ± 0·2	12	10·7
9	2·9	79,400	80	7·5	1840	2400	4·6	6·3	1·1 ± 0·2	10	6·0
10	3·55	83,400	—	6·3	2480	3500	6·3	9·2	1·3 ± 0·2	15	7·8
Mean ± S.D.				5·2 ± 1·5	1770 ± 380	2520 ± 660	9·3 ± 3·3	12·7 ± 4·5	1·4 ± 0·27	11·6 ± 4·1	12·9 ± 6·4

value of $70 \pm 15\ \Omega$ cm S.D., comparable to R_a values for other vertebrate neurones (Schanne, 1969). Our calculations used this average R_a value; R_a values of $50\ \Omega$ cm and $100\ \Omega$ cm yield R_m values 5–15% higher and (5–15% lower, respectively, than those reported here. Present evidence favours the hypothesis that dendritic terminals are closed and have a negligible conductance (Jack, Miller, Porter & Redman, 1971). Because dye may not

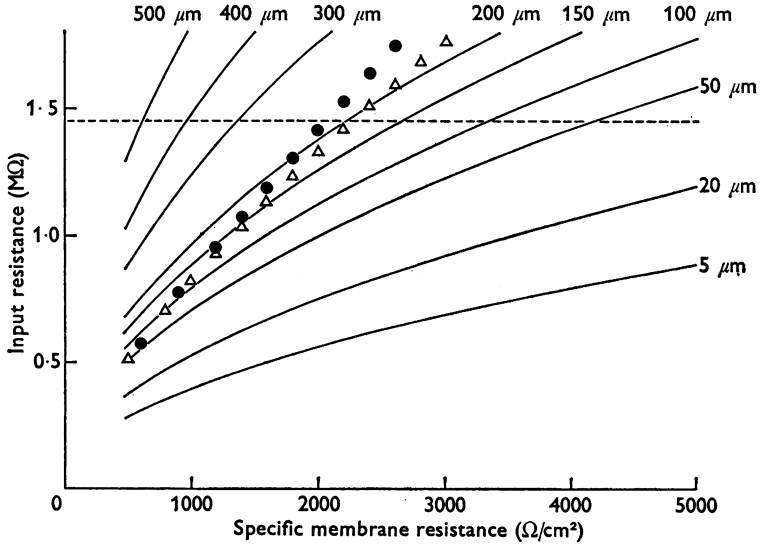

Text-fig 3. Calculated input resistance R_N (MΩ) as a function of specific membrane resistance R_m (Ω cm^2) for motoneurone 5, Table 1. Circles and triangles represent R_N values calculated from the detailed neuronal geometry using the closed-end and infinite-extension terminating conditions, respectively (see text). Dashed horizontal line marks 1·45 MΩ, the electrophysiologically measured value of R_N for this neurone. Continuous curves were calculated with the equivalent cylinder model of the dendritic tree, using values of the dendritic trunk parameter measured from neuronal geometry at the indicated distances from the soma.

reach the most distant dendritic terminals, R_m was determined for two extreme terminating conditions: (1) the closed-end approximation, which assumes that dendrites end at their most distal visible point and (2) the infinite-extension approximation, which uses a terminating conductance equal to the input conductance of a cable extending to infinity with a diameter equal to that of the most distal measured segment.

Text-fig. 3 plots the predicted input resistance R_N for a motoneurone (number 5 in Table 1) as a function of different assumed values for the uniform membrane resistance R_m. The calculated curves intersect the experimentally measured R_N value (1·45 MΩ) at an R_m of $2080\ \Omega$ cm^2

using the closed-end approximation (circles), or 2250 Ω cm² using the infinite-extension approximation (triangles). The actual R_m value assuming uniform R_m for the geometrical reconstruction of this neurone must lie between these limits. For ten motoneurones the mean values of R_m calculated using the closed-end and infinite-extension terminating conditions were 1770 Ω cm² and 2520 Ω cm², respectively (Table 1). Calculated R_m values show a small negative correlation with cell size ($r = -0{\cdot}24$, $P < 0{\cdot}025$, closed-end; $r = -0{\cdot}42$, $P < 0{\cdot}10$, infinite-extension).

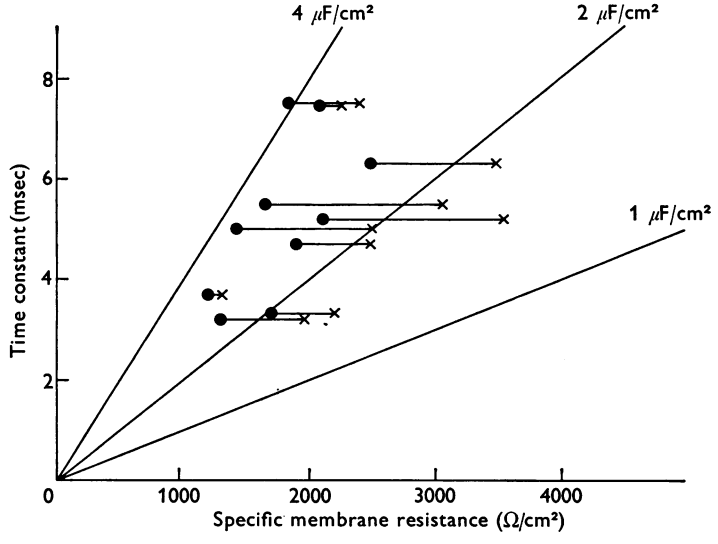

Text-fig. 4. Scatter plot of the electrophysiologically measured time constant τ_0 (msec) *vs.* the calculated value of specific membrane resistance R_m (Ω cm²) for ten motoneurones. τ_0 was measured from the slope of the final exponential decay assuming that the appropriate electrical geometry was a finite structure with open circuit termination of the dendrites (Rall, 1969). Filled circles represent R_m values calculated assuming closed-end dendritic terminations; × 's show R_m values determined assuming infinite extension (see text and Text-fig. 4). Horizontal lines connect the two R_m estimates for a particular motoneurone. Diagonal lines illustrate the theoretical relationships between τ_0 and R_m calculated assuming the indicated values of specific membrane capacity.

The continuous curves in Text-fig. 3 show the theoretical relationships between R_N and R_m calculated by approximating the dendritic tree as infinite equivalent cylinders (Rall, 1959), using values of the dendritic trunk parameter measured at the indicated distances from the soma of motoneurone 5. In this particular example, the values of R_m determined using the detailed neuronal geometry and the equivalent cylinder model coincide when the dendritic trunk parameter is measured 200 μm from

the soma. This 'coincident distance' varied from one motoneurone to another, however, so that the dendritic tree of the motoneurones studied here could not be approximated accurately merely by measuring the dendritic trunk parameter at some fixed distance from the soma.

The ratio of the combined input conductance of the dendrites to the input conductance of the soma, ρ, ranged from 4·6 to 16 (mean 9·3) for the closed-end approximation of the dendrites and from 6·3 to 21 (mean 12·7 for the infinite-extension model (Table 1). In calculating ρ the soma-dendrite junction was arbitrarily assumed to lie on the rapidly tapering base of the primary dendrites at the point where the rate of change of dendritic diameter became less than 10 % per micron.

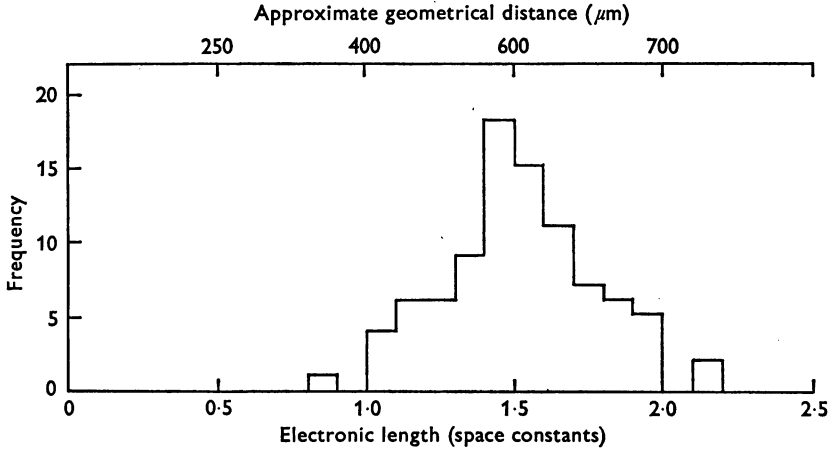

Text-fig. 5. Histogram of electrotonic lengths (space constants) calculated for the dendrites of motoneurone 5 using eqn. (3). Mean electrotonic length, 1·5 space constants.

The longest time constant, τ_0, of the voltage response to a current step input is equal to the product of R_m and the specific capacity, C_m. Thus, if C_m is constant from neurone to neurone, a plot of R_m vs. τ_0 for different neurones should be linear with a slope equal to C_m. The data plotted in Text-fig. 4 show C_m values between 1·5–4 μF/cm^2, with a mean value of 2·9 μF/cm^2 for the closed-end terminating condition (see above) and 2·1 μF/cm^2 for the infinite-extension condition.

Electrotonic lengths of dendrites. Our morphological measurements were sufficiently detailed to allow calculation of the electrotonic length L of every dendrite of each of the ten motoneurones in Table 1, using the equation (Rall, 1959, 1962):

$$L = \int_0^{x_1} 1/\lambda \, dx, \tag{3}$$

where x_1 is the geometrical distance from the soma to a terminal dendritic branch and λ is the space constant of a dendritic segment,

$$\lambda = \tfrac{1}{2}\sqrt{d}\sqrt{(R_m/R_a)}.$$

L ranged from 0·8 to 2·2 space constants (mean 1·4) for all the dendrites studied (dendritic terminals were 300–800 μm from the soma). The average electrotonic length of the dendrites of a given motoneurone ranged from 1·1 to 1·5 space constants (Table 1). These calculated average L values agree quite well with previous electrophysiological estimates of L (Burke & ten Bruggencate, 1971), arguing that most of the distal dendritic branches were included in our sample, and that the dendrites terminate in closed ends. Text-fig. 5 is a histogram of the calculated electrotonic lengths from the soma to each of the ninety terminal dendritic branches in motoneurone 5.

Text-fig. 6 plots the dendritic trunk parameter ($\Sigma d^{\frac{3}{2}}$) as a function of

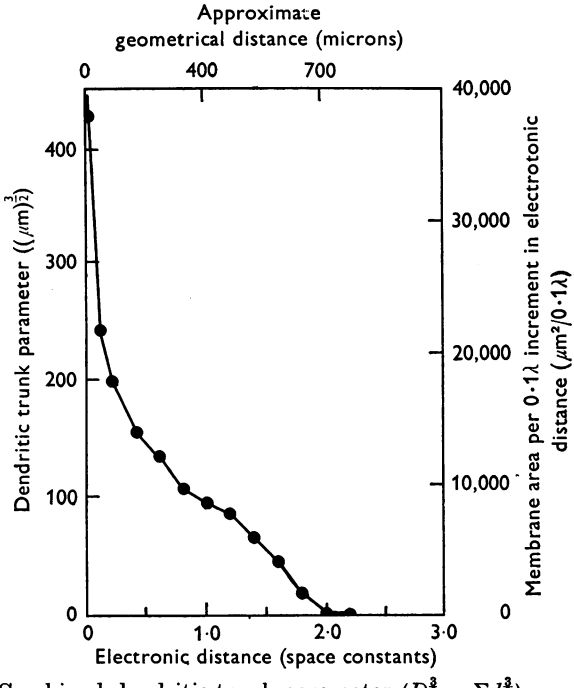

Text-fig. 6. Combined dendritic trunk parameter ($D^{\frac{3}{2}} = \Sigma d^{\frac{3}{2}}$) as a function of electrical distance from the soma in motoneurone 5. Because the derivative of membrane area with respect to electrotonic length is directly proportional to $D^{\frac{3}{2}}$ (eqn. (4)), this plot also gives the fraction of dendritic area at various electrotonic distances from the soma, as indicated by the right-hand scale. Left-hand ordinate: $\mu m^{\frac{3}{2}}$, right-hand ordinate: $\mu m^2/0{\cdot}1\lambda$, abscissa: space constants. Electrotonic distance was calculated assuming an R_m value of 2000 Ω cm^2.

electrotonic distance from the soma for motoneurone 5. The progressive decrease in $\Sigma d^{\frac{3}{2}}$ during the proximal 0·8 space constant is primarily due to tapering of the individual dendrites between branch points (Pl. 1). Beyond 0·8 space constant an increasingly large portion of the decrease in $\Sigma d^{\frac{3}{2}}$ results from the termination of dendritic branches.

Eqn. (4) shows that the increment in membrane area for a small increment in electrotonic length (ΔZ) is proportional to the value of the combined dendritic trunk parameter at the given electrical distance L_1:

$$\left.\frac{\partial A_T}{\partial Z}\right|_{L_1} = \sum_j \left(\frac{\partial A_j}{\partial x} \cdot \frac{dX}{dZ}\right)\Bigg|_{L_1} = \sum_j \pi d_j \lambda_j = \frac{\pi}{2}\sqrt{\left(\frac{R_m}{R_a}\right)} \sum_j d_j^{\frac{3}{2}}, \tag{4}$$

where A_T at L_1 is the cumulative membrane area between the soma and L_1 expressed as a function of electrical length; A_j is the same area function for a single dendritic branch; d_j is the diameter of the jth branch at L_1; and x is geometrical length. This relationship holds for any dendritic geometry, and is implicit in eqn. (21) of Rall (1962).

Accordingly, Text-fig. 6 also plots the relative amount of membrane area at different electrotonic distances from the soma (see right-hand scale). It is evident that membrane area decreases steeply with electrical distance. Thus, even if the density of synaptic endings were constant over the entire neuronal membrane, only a small fraction of the endings would be electrically distant from the soma. In fact, Ia afferent terminals are less dense on distant than on proximal dendrites (Conradi, 1969), suggesting that even fewer synapses are electrically distant from the soma than would be predicted solely on the basis of dendritic membrane area. By multiplying our values of membrane area at various electrotonic distances from the soma (Text-fig. 6) by Conradi's values for the percentage of Ia synapses at the approximately corresponding geometrical distances, we obtained a rough estimate of the distribution of Ia synapses with electrotonic distance from the soma. This distribution agrees approximately with that predicted from the shape of Ia e.p.s.p.s by Jack *et al.* (1971), both distributions showing fewer than 10% of the Ia synapses located more than 1·5 space constants from the soma.

Predicting the transient voltage response at the soma. Tapering of the dendritic tree (Pl. 1, Text-fig. 6) should have predictable effects on the electrical responses of the neurone. In an attempt to obtain electrical evidence for dendritic tapering, we calculated the impulse response, $h(t)$, predicted for a detailed, tapering neuronal geometry and for non-tapering equivalent cylinders (Text-fig. 7), and compared these calculated responses to the derivative of the measured voltage response to a current step applied at the soma (Burke & ten Bruggencate, 1971). Calculations of the predicted impulse responses used the Fourier techniques described in Methods and

the Appendix. A peeling procedure used by Rall (1969), Nelson & Lux (1960) and Burke & ten Bruggencate (1971) was employed to express both the calculated impulse responses and the derivative of the measured step response as a series of exponential components of the following form:

$$h(t) = h_0 e^{-t/\tau_0} + h_1 e^{-t/\tau_1} + \ldots + h_n e^{-t/\tau_n}, \quad (5)$$

where h_0 and τ_0 are the amplitude and time constant, respectively, of the slowest term in the series ($\tau_0 = R_m C_m$).

Unfortunately, our electrical measurements were not sufficiently accurate to distinguish between the tapering and nontapering models. The use of single relatively high resistance electrodes to pass current and record voltage responses, and the negative capacitance feed-back system probably produced a systematic distortion of the transient responses, especially their earlier portions. The ratio of the two slowest time constants, τ_0/τ_1, averaged 5·2, in approximate agreement with the τ_0/τ_1 ratios predicted from the tapering neuronal geometry, but also agreeing with the τ_0/τ_1 ratios calculated for a nontapering equivalent cylinder with an electrotonic length intermediate between the average and the longest measured electrotonic lengths of the neurone's dendrites.

M. Goldstein & W. Rall used a different calculation technique to predict the impulse response for a single equivalent core conductor with two exponential tapers fitting the $\Sigma d^{\frac{3}{2}}$ *vs.* electrotonic distance relationship measured for motoneurone 5 (Text-fig. 6). They calculated a time constant ratio, τ_0/τ_1, in approximate agreement with the ratio we determined using the detailed neuronal geometry (personal communication).

The nontapering equivalent cylinder and detailed geometry models predict considerably different amplitude ratios h_0/h_1: the detailed geometry gives h_0/h_1 values of approximately 1, whereas the equivalent cylinder model predicts a ratio of 0·5, regardless of the electrotonic length of the cylinder. The measured values of h_0/h_1 for neurones in this study averaged 0·66, but these amplitude measurements are subject to consider-

Legend to Text-fig. 7

Text-fig. 7. Computer calculated transient responses for motoneurone 5 (Table 1). *A*, current-clamp impulse responses. *B*, voltage-clamp current transient responses. In both *A* and *B* the continuous line is calculated response for a uniform soma and dendritic membrane resistance of 2000 Ω cm²; dashed line is calculated response for a dendritic membrane resistance of 8000 Ω cm² and a soma membrane resistance of 294 Ω cm²; and dotted line is calculated response for a nontapering equivalent cylinder model with a uniform membrane resistance of 2000 Ω cm². The abscissa is normalized so that the three models give the same values for their longest observed time constant.

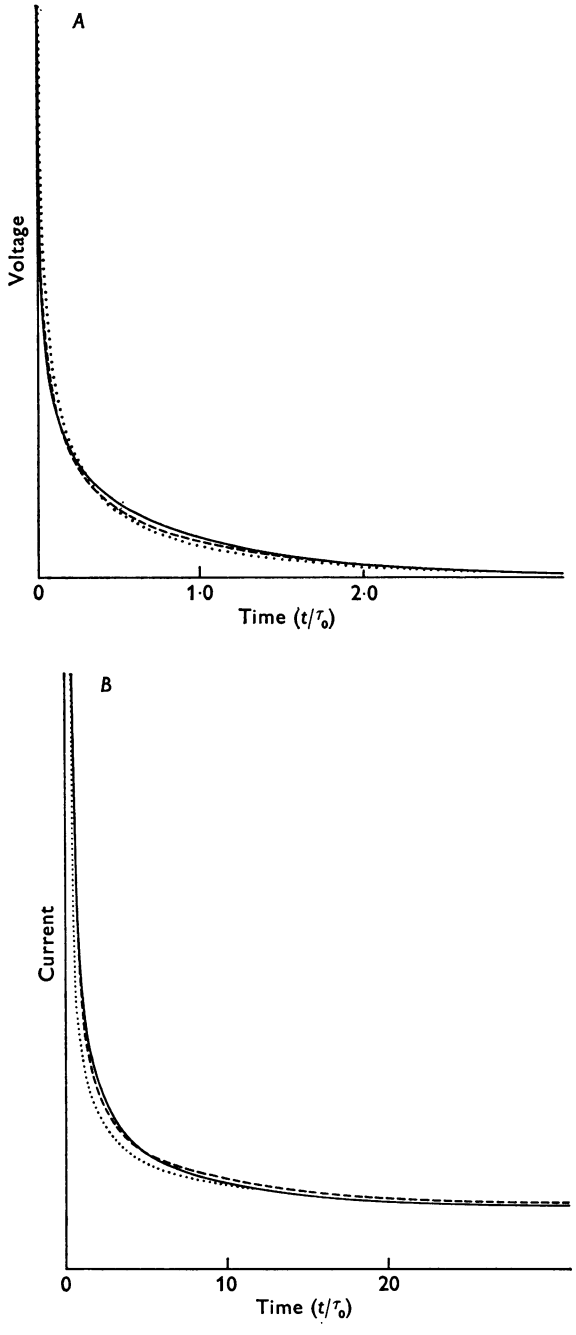

Text-fig. 7. For legend see opposite page.

able error from imperfections in the shape of the current pulse and in the capacity compensation system of the voltage recording amplifier. However, measurements of voltage-clamp transients made with a better recording system (employing separate current and voltage electrodes) for a different sample of motoneurones (not injected with dye) were also best fitted assuming an impulse response with an h_0/h_1 ratio of about 0·7. The fact that our measured h_0/h_1 ratios fell between the values predicted by the tapering and nontapering models might argue for a degree of tapering less than seemed evident from our anatomical measurements, but in fact amplitude ratios measured to date are probably too inaccurate to define the degree of tapering in the dendritic tree.

DISCUSSION

The geometry and electrical properties of the same motoneurones have been measured in order to calculate R_m and C_m for a core conductor model of the cells. The calculated parameters represent effective values, averaging out possible local nonuniformities with spatial extents short compared to the electrical space constant. Use of the core conductor model is based on assumptions expressed in other studies (Rall, 1959; Jack & Redman, 1971).

Dye injection and histological procedures. Artifactual alteration of neuronal dimensions could significantly affect calculations of membrane parameters, since R_m varies with the measured values of dendritic diameter. Comparison of dye-injected motoneurones with adjacent uninjected motoneurones suggested that dye injection did not distort general neuronal morphology unless sustained currents exceeding 100 nA were used. Similarly, frog muscle fibres injected under direct observation showed no detectable change in diameter unless currents (> 40 nA) sufficient to produce local contraction were used (unpublished observation). Pruves & McMahan (1972) reported little or no gross morphological distortion of Procion dye-injected leech motoneurones, but did see obvious changes at the ultrastructural level (e.g. swelling of mitochondria and endoplasmic reticulum, and altered staining of some cellular constituents). The paraformaldehyde fixative solution used in this study was hypertonic (final buffer osmolarity 450 m-osmole) and could have caused some cell shrinkage, yielding an underestimate of R_m. However, distances between dye reference markers in spinal cord did not change during fixation. Likewise, no alteration in neuronal dimensions was observed upon transferring sections into the glycerol mounting solution. The absence of gross changes in dimension suggests, but does not prove, that there was no significant swelling or shrinkage in single motoneurones.

Previous studies estimated R_m using geometrical measurements from alcohol-dehydrated motoneurones, but only Lux *et al.* (1970) attempted to correct for shrinkage. Shrinkage due to alcohol dehydration may be one reason why earlier studies based on Golgi-stained preparations gave lower values of R_m.

We observed a significant decrease in the dendritic trunk parameter throughout the length of the dendritic tree in most dye-injected motoneurones, in contrast with the report by Lux *et al.* of little decrease at distances beyond 50 μm in motoneurones injected with radioactive glycine. These discrepant results may be due to errors in one or both experimental methods. It is possible that the tapering between branch points is an artifact produced by dye diffusion gradients. Such gradients could also cause premature loss of fine dendritic branches. However, when such gradients were deliberately enhanced by fixing the preparation immediately after dye injection, there was no systematic increase in measured tapering, and neurones given twelve hours of post-injection diffusion time still showed tapering. Dendritic fluorescence was usually many times higher than the background level, making artifactual loss of dendrites greater than 1 μm in diameter extremely unlikely, but it is conceivable that some small dendritic branches became blocked and did not fill with dye at all. On the other hand, Lux *et al.* may have overestimated the diameter of the smaller more distal dendritic branches in their autoradiographs due to scattering of tritium beta particles (Hill, 1962). Further improvements of both methods, perhaps in combination with electron microscopy, will be necessary to determine the actual degree of tapering in individual motoneurones and in different populations of motoneurones (cf. Kellerth, 1973).

Calculation of passive membrane properties. Models of the electrical behaviour of neuronal membranes usually include an unchanging membrane capacitance and two classes of ionic conductances: (1) instantaneous passive leakage conductances, and (2) active conductances that are a function of time and voltage. If the values of R_m calculated in this study are to estimate the passive instantaneous conductance of the soma and dendrites, R_N must be measured where the slope of the voltage–current relationship is constant. Previous studies indicate that the voltage–current curve is approximately linear between the resting potential and threshold (Araki & Terzuolo, 1962; Nelson & Frank, 1967; see however, Ito & Oshima, 1965), and our measurements confirmed this. The 1–5 nA depolarizing current used here to estimate R_N produced voltage changes within this passive linear range.

In calculating the specific membrane parameters of the motoneurone it is necessary to take into account the geometrical properties of the dendritic tree. Rall (1959) developed iterative procedures for calculating R_m that

could be applied to any dendritic geometry, but in most previous studies the dendrites have been approximated by finite or infinite equivalent cylinders (Rall, 1959; Kernell, 1966; Lux *et al.* 1970). Our geometrical measurements did not justify this approximation because in most motoneurones the dendritic trunk parameter decreased with distance from the soma (Text-fig. 6). Thus we calculated the relation between specific membrane parameters and the measured input impedance at the motoneuronal soma by applying Rall's original iterative methods (extended to the transient case, see Appendix) to a detailed segmented model of the dendritic tree.

Synaptic activity can markedly reduce the effective values of R_N and R_m (Smith, Wuerker & Frank, 1967; Barrett & Crill, 1974). The anaesthetic levels used here have no direct effect on R_N (Weakly, 1969), but the reduction in incoming synaptic activity produced by combined anaesthesia and paralysis probably results in R_N and R_m values greater than the effective values in alert, active preparations.

The calculations reported here assumed a uniform R_m. However, even if the soma had an infinite R_m, the calculated dendritic R_m would be only 20% lower than the uniform R_m value. Thus, regardless of whether R_m is uniform over both dendrites and soma, the values calculated assuming uniformity must estimate the lower bound of dendritic R_m. In an attempt to place an upper bound on dendritic R_m, current-step and voltage-clamp transient responses were calculated assuming various non-uniform distributions of R_m. However, dendritic R_m could exceed 8000 Ω cm^2 (in this case, somatic R_m would be 240 Ω cm^2) before the predicted, time-normalized transient (since $\tau_0 \neq R_m C_m$ when R_m is not uniform, time normalization was done on the basis of computed τ_0 values) response becomes significantly discrepant from our transient response data. (The major differences between the calculated transient responses occur in their early time course, where our measurements were subject to systematic error.) Thus, the major positive accomplishment of this study was to place a lower limit of about 1800 Ω cm^2 on the average specific resistance of the dendritic membrane in motoneurones of anaesthetized paralysed cats. This lower bound on dendritic R_m is important in the calculations of the functional role of dendritic synapses presented in the following paper (Barrett & Crill, 1974).

The values calculated for specific membrane capacitance (2–3 μF/cm^2) are higher than the value of 1 μF/cm^2 measured for crustacean and squid axons (Hodgkin & Rushton, 1946; Hodgkin, Huxley & Katz, 1952) and generally accepted as a standard value for biological membranes. Our higher calculated values of C_m could be due to underestimation of R_m, caused for example by loss of distant dendritic branches or by cell shrink-

age. Nonuniformities in R_m could also cause errors in the value of C_m estimated by dividing the average R_m by the longest time constant of the step response. For example, in the case discussed above (dendritic R_m 8000 Ω cm², somatic R_m 240 Ω cm²) this calculation method would overestimate C_m by a factor of two. The value of C_m can also be overestimated if membrane folding is not taken into account (discussed by Gorman & Mirolli, 1972), but electron micrographs of cat motoneurones show very few membrane folds or spines (Conradi, 1969).

On the other hand, it is possible that C_m for the motoneuronal membrane is greater than 1 μF/cm². Several studies of vertebrate neurones calculate higher values of C_m, for example, 3 and 1·6 μF/cm² in cat and rat superior cervical ganglion neurones, respectively (Skok, 1968; Sacchi & Casella, 1970) and 1·5–5 μF/cm² in pyramidal neurones of cat motor cortex (Lux & Pollen, 1966). Woodbury, White, Mackey, Hardy & Chang (1970) point out that a small increase in the protein content of the cell membrane could significantly increase C_m, because the dielectric constants of proteins are greater than those of lipids.

APPENDIX

Calculating the impulse response of the soma

This section derives the basic cable equation used to calculate the input impedance of a dendritic segment at a given frequency ω from the geometrical and electrical properties of the segment and its termination impedance. Calculations for all the dendritic segments are combined and used to determine the complex input impedance of the soma, from which the impulse response of the soma is predicted.

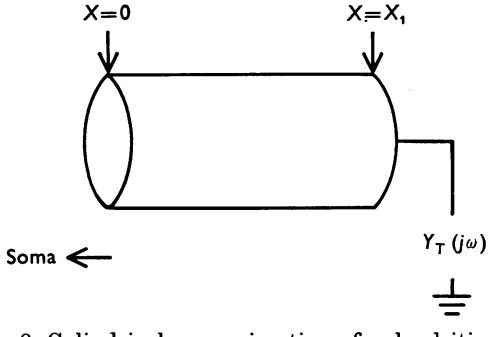

Text-fig. 8. Cylindrical approximation of a dendritic segment.

The dendrites are divided into short segments, each approximated as a core-conducting membrane cylinder (Text-fig. 8) with length Δx, time constant τ ($\tau = R_m C_m$), diameter d, axoplasmic resistivity R_a (70 Ω cm),

space constant λ [$\lambda = \frac{1}{2}\sqrt{d}\sqrt{(R_m/R_a)}$], and terminating complex admittance $Y_T(j\omega)$ (equal to the admittance seen from x_1 looking into the distal adjoining segment). The cable equation for the membrane cylinder is

$$\frac{\lambda^2 \partial^2 V(x,t)}{\partial x^2} = \tau \frac{\partial V(x,t)}{\partial t} + V(x,t). \tag{6}$$

Taking the Fourier transform of eqn. (6) with respect to time yields

$$\frac{d^2 \hat{V}(x,j\omega)}{dx^2} = \hat{V}(x,j\omega)\left(\frac{1+j\omega\tau}{\lambda^2}\right)$$

whose general solution is:

$$\hat{V}(x,j\omega) = A_1 e^{\gamma x} + A_2 e^{-\gamma x}, \tag{7}$$

where

$$\gamma = \frac{\sqrt{(1+j\omega\tau)}}{\lambda}.$$

The transform of the current leaving the cylinder at x_1 equals the product of the transforms of the terminating admittance $Y_T(j\omega)$ and the voltage at x_1:

$$\hat{I}(x_1,j\omega) = -\frac{1}{R_a}\frac{d\hat{V}(x,j\omega)}{dx}\bigg|_{x_1} = Y_T(j\omega)\,\hat{V}(x_1,j\omega). \tag{8}$$

The ratio of the constants A_1 and A_2 in eqn. (7) is given by

$$\frac{A_2}{A_1} = e^{2\gamma x_1}\left\{\frac{\gamma + Y_T(j,\omega)\,R_a}{\gamma - Y_T(j,\omega)\,R_a}\right\}. \tag{9}$$

Similarly, the transform of the current flowing into the cylinder at its proximal end ($x = 0$) equals the product of the input admittance transform $Y_{in}(j\omega)$, times the transform of the voltage at $x = 0$;

$$\hat{I}(x=0,j\omega) = -\frac{1}{R_a}\frac{d\hat{V}(x,j\omega)}{dx}\bigg|_{x=0} = Y_{in}(j\omega)\,\hat{V}(0,j\omega). \tag{10}$$

Simultaneous solution of eqns. (7) and (10) for the transform of the input admittance of the cylinder $Y_{in}(j\omega)$ gives:

$$Y_{in}(j\omega) = \frac{\gamma}{R_a}\left\{\frac{A_2/A_1 - 1}{A_2/A_1 + 1}\right\}. \tag{11}$$

Substituting in eqn. (11) the value of (A_2/A_1) from eqn. (9) yields:

$$Y_{in}(j\omega) = \frac{\sqrt{1+j\omega\tau}}{R_a\lambda} \times \left\{\frac{\left[\exp\left(\frac{2\Delta x}{\lambda}\sqrt{(1+j\omega\tau)}\right)\right][\sqrt{(1+j\omega\tau)} + R_a\lambda Y_T] + R_a\lambda Y_T - \sqrt{(1+j\omega\tau)}}{\left[\exp\left(\frac{2\Delta x}{\lambda}\sqrt{(1+j\omega\tau)}\right)\right][\sqrt{(1+j\omega\tau)} + R_a\lambda Y_T] - R_a\lambda Y_T + \sqrt{(1+j\omega\tau)}}\right\}. \tag{12}$$

The complex terminating admittance $Y_T(j\omega)$ may be written as the sum of real and imaginary parts:

$$Y_T = \alpha(\omega) + j\beta(\omega). \tag{13}$$

Substituting eqn. (13) for $Y_T(j\omega)$ in eqn. (12) gives an expression for $Y_{in}(j\omega)$ that can be separated into real and imaginary parts:

$$Y_{in}(j\omega) = P(\alpha, \beta, \tau, \lambda, x_1, \omega) = jQ(\alpha, \beta, \tau, \lambda, x_1, \omega), \tag{14}$$

where

$$P(\alpha, \beta, \tau, \lambda, x_1, \omega) = \frac{1}{R_a\lambda}\left(\frac{CG+HD}{G^2+H^2}\right),$$

$$Q(\alpha, \beta, \tau, \lambda, x_1, \omega) = \frac{1}{R_a\lambda}\left(\frac{DG-CH}{G^2+H^2}\right),$$

$$C = a(A + R_a\lambda\alpha - a) - b(B + R_a\lambda\beta - b),$$

$$D = b(A + R_a\lambda\alpha - a) + a(B + R_a\lambda\beta - b),$$

$$G = A - R_a\lambda\alpha - a,$$

$$H = B - R_a\lambda\beta + b,$$

$$A = \exp\left(\frac{2x_1a}{\lambda}\right)\left[(a + R_a\lambda\alpha)\cos\left(\frac{2x_1b}{\lambda}\right) - (b + R_a\lambda\beta)\sin\left(\frac{2x_1b}{\lambda}\right)\right],$$

$$B = \exp\left(\frac{2x_1a}{\lambda}\right)\left[(a + R_a\lambda\alpha)\sin\left(\frac{2x_1b}{\lambda}\right) + (b + R_a\lambda b)\cos\left(\frac{2x_1b}{\lambda}\right)\right],$$

$$a = \sqrt{\left(\frac{\sqrt{(1+\omega^2\tau^2)}+1}{2}\right)}, \quad b = \sqrt{\left(\frac{\sqrt{(1+\omega^2\tau^2)}-1}{2}\right)}.$$

At a given frequency ω_1 only two numbers $\alpha(\omega_1)$ and $\beta(\omega_1)$ are required to specify the input admittance Y_{in} of a given segment k. Since Y_{in} for segment k is the terminating admittance, Y_T, of the next more proximal segment $k+1$, the α and β values specifying Y_{in} for segment k also specify the value of Y_T needed to calculate Y_{in} for segment $k+1$ at ω_1. Calculations start at the most distal visible dendritic tip, assuming either sealed or infinite-cylinder termination (see Results), and proceed iteratively toward the soma. At branch points the terminating admittance of the parent dendritic trunk equals the sum of the input admittances of the daughter branches. The input admittance at the soma is the sum of the input admittances of all the dendrites added in parallel and the input admittance of the soma calculated from its shape. The input impedance at the soma is the reciprocal of the soma input admittance.

We thank Drs W. L. Hardy, B. Hille, C. F. Stevens and J. W. Woodbury for helpful discussion and criticism, Dr T. Kehl and his staff for computer facilities and

assistance. Dr M. Heath for help in calculating the complex input admittance of the neurone and Dr E. Barrett for careful reading and editing of the manuscript. The work was supported by USPHS grants GM 00739, NS 09787, Fr 00374 and NS 05934.

REFERENCES

AITKEN, J. T. & BRIDGER, J. E. (1961). Neuron size and neuron population density in the lumbosacral region of the cat's spinal cord. *J. Anat.* **95**, 38–53.

ARAKI, T. & TERZUOLO, C. A. (1962). Membrane currents in spinal motoneurons associated with the action potential and synaptic activity. *J. Neurophysiol.* **25**, 772–789.

BARRETT, J. N. (1973). Determination of neuronal membrane properties using intracellular staining techniques. In *Intracellular Staining Techniques in Neurobiology*, ed. KATER, S. B. & NICHOLSON, C. Berlin: Springer-Verlag.

BARRETT, J. N. & CRILL, W. E. (1971*a*). Efficacy of distant dendritic synapses in cat motoneurones. *Fedn Proc.* **30**, 323.

BARRETT, J. N. & CRILL, W. E. (1971*b*). Specific membrane resistivity of dye-injected motoneurons. *Brain Res.* **28**, 556–561.

BARRETT, J. N. & CRILL, W. E. (1974). The influence of dendritic location and membrane properties on the effectiveness of synapses on cat motoneurones. *J. Physiol.* **239**, 325–345.

BARRETT, J. N. & GRAUBARD, K. (1970). Fluorescent staining of cat motoneurons *in vivo* with beveled micropipettes. *Brain Res.* **18**, 565–568.

BURKE, R. E. & TEN BRUGGENCATE, G. (1971). Electrotonic characteristics of alpha motoneurones of varying size. *J. Physiol.* **212**, 1–10.

CONRADI, S. (1969). On motoneuron synaptology in adult cats. *Acta physiol. scand.* suppl. 332.

COOMBS, J. S., CURTIS, D. R. & ECCLES, J. C. (1959). The electrical constants of the motoneurone membrane. *J. Physiol.* **145**, 505–528.

FRANK, K. & FUORTES, M. G. F. (1956). Stimulation of spinal motoneurones with intracellular electrodes. *J. Physiol.* **134**, 451–470.

GORMAN, A. L. F. & MIROLLI, M. (1972). The geometrical factors determining the electrotonic properties of a molluscan neurone. *J. Physiol.* **227**, 35–49.

HILL, D. K. (1962). Resolving power with tritium autoradiographs. *Nature, Lond.* **194**, 831–832.

HODGKIN, A. L., HUXLEY, A. F. & KATZ, B. (1952). Measurement of current-voltage relations in the membrane of the giant axon of *Loligo*. *J. Physiol.* **116**, 424–448.

HODGKIN, A. L. & RUSHTON, W. A. H. (1946). The electrical constants of a crustacean nerve fibre. *Proc. R. Soc.* B **133**, 444–479.

ITO, M. & OSHIMA, T. (1965). Electrical behaviour of the motoneurone membrane during intracellularly applied current steps. *J. Physiol.* **180**, 607–635.

JACK, J. J. B., MILLER, S., PORTER, R. & REDMAN, S. J. (1971). The time course of minimal excitatory post-synaptic potentials evoked in spinal motoneurones by Group Ia afferent fibres. *J. Physiol.* **215**, 353–380.

JACK, J. J. B. & REDMAN, S. J. (1971). The propagation of transient potentials in some linear cable structures. *J. Physiol.* **215**, 283–320.

KELLERTH, J. (1973). Intracellular staining of cat spinal motoneurones with Procion yellow for ultrastructural studies. *Brain Res.* **50**, 415–418.

KERNELL, D. (1966). Input resistance, electrical excitability, and size of ventral horn cells in cat spinal cord. *Science, N.Y.* **152**, 1637–1640.

LUX, H. D. & POLLEN, D. A. (1966). Electrical constants of neurones in the motor cortex of the cat. *J. Neurophysiol.* **29**, 207–220.

LUX, H. D., SCHUBERT, P. & KREUTZBERG, G. W. (1970). Direct matching of morphological and electrophysiological data in cat spinal motoneurons. In *Excitatory Synaptic Mechanisms*, Proc. of the Fifth International Meeting of Neurobiologists, ed. ANDERSON, P. & JANSEN, J. K. S. Oslo: Universitetsforlaget.

NELSON, P. G. & FRANK, K. (1967). Anomalous rectification in cat spinal motoneurons and effect of polarizing currents on excitatory post-synaptic potential. *J. Neurophysiol.* **30**, 1097–1113.

NELSON, P. G. & LUX, H. D. (1970). Some electrical measurements of motoneuron parameters. *Biophys. J.* **10**, 55–73.

NORMAN, R. S. (1972). Cable theory for finite length dendritic cylinders with initial and boundary conditions. *Biophys J.* **12**, 24–45.

PERRI, V., SACCHI, O. & CASELLA, C. (1970). Electrical properties and synaptic connections of the sympathetic neurone in the rat and guinea-pig superior cervical ganglion. *Pflügers Arch. ges. Physiol.* **314**, 40–54.

PURPLE, R. L. (1964). The integration of excitatory and inhibitory influences in the eccentric cell in the eye of *Limulus*. Ph.D. Dissertation, The Rockefeller Institute.

PURVES, D. & MCMAHAN, U. J. (1972). The distribution of synapses on a physiologically identified motor neuron in the central nervous system of the leech: an electron microscope study after the injection of the fluorescent dye Procion Yellow. *J. cell Biol.* **55**, 205–220.

RALL, W. (1959). Branching dendritic trees and motoneuron membrane resistivity. *Expl Neurol.* **1**, 491–527.

RALL, W. (1962). Theory of physiological properties of dendrites. *Ann. N.Y. Acad. Sci.* **96**, 1071–1092.

RALL, W. (1969). Time constants and electrotonic length of membrane cylinders and neurons. *Biophys. J.* **9**, 1483–1508.

ROJAS, E., BEZANILLA, F. & TAYLOR, R. E. (1970). Demonstration of sodium and potassium conductance changes during a nerve action potential. *Nature, Lond.* **225**, 747–748.

SCHANNE, O. F. (1969). Measurement of cytoplasmic resistivity by means of the glass microelectrode. In *Glass Microelectrodes*, ed. LAVALLÉE, M., SCHANNE, O. F. & HÉBERT, N. C. New York: Wiley.

SKOK, V. I. (1968). Electrophysiological properties of sympathetic ganglia. Dissertation, Kiev. U.S.S.R. (in Russian). Cited in *Physiology of Autonomic Ganglia*, SKOK, V. I., pp. 76–79. Japan: Nijon Koishu Pub.

SMITH, T. G., WUERKER, R. B. & FRANK, K. (1967). Membrane impedance changes during synaptic transmission in cat spinal motoneurones. *J. Neurophysiol.* **30**, 1072–1096.

STRETTON, A. O. W. & KRAVITZ, E. A. (1968). Neuronal geometry: determination with a technique of intracellular dye injection. *Science, N.Y.* **162**, 132–134.

WEAKLY, J. N. (1969). Effect of barbiturates on 'quantal' synaptic transmission in spinal motoneurones. *J. Physiol.* **204**, 63–77.

WESTRUM, L. E. & LUND, R. D. (1966). Formalin perfusion for correlative light- and electron microscopical studies of the nervous system. *J. cell Sci.* **1**, 229–238.

WOODBURY, J. W., WHITE, S. H., MACKEY, M. C., HARDY, W. L. & CHANG, D. B. (1970). Bioelectrochemistry. In *Electrochemistry*, ed. EYRING, H., JOST, W. & HENDERSON, D. New York: Academic Press.

EXPLANATION OF PLATE

PLATE 1

Dendritic tapering in a Procion-dye injected motoneurone. The illustrated decrease in diameter with distance from the soma is typical of most dendrites observed in this study. Two photographs were combined to keep the dendrite in focus. Scale 100 μm.